Observer and Robust H_∞ Control of a 2-DOF Piezoelectric Actuator Equipped with Self-Measurement

Omar Aljanaideh[1], and Micky Rakotondrabe[2], *member, IEEE*

Abstract— This paper introduces a dynamic observer in order to estimate the displacement in a 2-DOF piezoelectric actuator (piezoactuator) devoted to precise positioning and equipped with static self-measurement circuit. Then, the estimated displacement derived by the suggested observer is used as feedback for a robust H_∞ controller. The 2-DOF piezoactuator is characterized by strong cross-couplings which are accounted for in the observer and in the feedback controller. Experimental results demonstrate the efficiency of the observer as well as the H_∞ controller. The approach is very interesting for piezoelectric systems where it is difficult to implement sensors for feedback, such as in precise positioning applications at the small scale where measurement technology is still challenging.

Observer, H_∞ Control, Self-Measurement

I. INTRODUCTION

Piezoelectric actuators play a key role in applications that require precise positioning. These actuators are able to deliver a quick and highly resolute output displacement that is convenient for microrobotics [1], micromanipulation [2], [3], atomic force microscopy [4] and data-storage [5] applications. The implementation of these actuators in real system is often limited to a narrow operating range due to the presence of vibrations and nonlinear effects as well as due to internal or external disturbances. This necessitates synthesizing feedback control techniques in order to improve their performance in real-time system [6]. However, the application of feedback control techniques require expensive feedback sensors that can deliver precise information about the output displacement in nanometric level resolution. Such sensors are generally bulky and thus reserve large space which is not available in some microsystems environment [7]. In addition, integration of multi-degree of freedom piezoactuators requires installation of many feedback sensors that can measure the displacement in each axis which is a challenging task. Feedforward control have been developed in order to compensate for the lack of convenient sensors in piezoelectric systems [8]–[12] but the main limitation of such architecture is the lack of robustness.

[1]Omar Aljanaideh, Senior Control Engineer at ASML-HMI, San Jose, 95131 CA USA omar.aljanaideh@asml.com

[2]Micky Rakotondrabe is with FEMTO-ST Institute, Université Bourgogne Franche-Comté, CNRS, Besançon France mrakoton@femto-st.fr

Self-measurement technique is considered as a reliable solution where these challenges exist. This approach employs the actuator itself as a sensor that can calculate the deflection and/or the output force based on the reversibility property of the actuator material. More precisely, for piezoactuators case, an external electrical circuit is employed to amplify the electrical charge appearing on the piezoelectric electrodes during its deformation and due to piezoelectric effect. The amplified electrical charge, which is an exploitable voltage, is used among the other available signals (the driving voltage of the actuator) as information to an observer in order to estimate the displacement and/or the force.

Self-measurement principle was pioneered by J. Dosch et al in [13], where the vibration of a piezoactuator was controlled without using feedback sensor. Several attempts have been carried out to employ the self-measurement technique for control purposes [14], [15], [16]. Although these schemes have been proposed and applied to adapt the self-measurement with different flexible structures, they lack the long-term measurements (i.e. static and low frequency signals measurements) as well as the consideration of hysteresis and creep nonlinearities [17]. Moreover, these methodologies consider only one degree of freedom where the cantilevered actuator moves only in one direction. However, several microsystems employ multi-degree of freedom (DOF) structures such as piezoelectric tubes and 2-DOF multimorph cantilevered actuators, which require estimating output displacement in more than one axis.

In the previous works [18], a self-measurement technique was developed to estimate the force at low frequency regime and the output displacement of a piezoactuator at low and high frequency regime. The observer was coupled with a robust H_∞ displacement feedback control to demonstrate the benefits of this approach. In [19]–[21], another observer has been proposed for the same actuator in order to estimate the force, the displacement and the state, all in low and high frequency regimes. These techniques were however used to estimate the displacement of 1-DOF actuator that exhibits displacement in one axis only.

Multi-DOF piezoactuators that show the output displacement in different axes necessitate implementation of multi-DOF observer that can estimate the displacement of the actuator in different axes. In a recent study [22], a 2-DOF self-measurement observer technique was suggested to estimate the static (steady-state) output displacement of a 2-DOF piezoactuator in two different axes. The suggested observer, however, ignores the dynamic properties of the actuator as well as the

dynamics of coupling effects between both axes. Ignoring these properties contributes significant errors in estimating the transient response of the actuator, and limits the application of the observer to the static displacement of the actuator which is not consistent with (dynamic) feedback control. In this paper, we presents a 2-DOF self-measurement observer that accounts for the dynamics of a 2-DOF actuator and the coupling effects between the two axes. The advantage of the proposed dynamic self-measurement is that it is usable for feedback control. Hence, we develop a H_∞ robust controller for the actuator by using the resulting estimate signal. The controller is synthesized to enhance the tracking performance of the actuator and to insure handling the disturbance effects that piezoactuators experience in miniaturized systems.

The rest of the paper is organized as follows. Section-II is devoted to the presentation of the experimental setup and to a remind of the static self-measurement. Then, in section-III, we present the dynamic observer that permits to the self-measurement to estimate the output displacement of the actuator at low and high frequency regime. Experimental validation is also presented in the same section. In section-IV, a H_∞ controller is synthesized and tested to the 2-DOF piezoactuator by using the 2-DOF dynamic self-measurement as feedback. Finally, conclusion and some perspectives are presented in section-V.

II. EXPERIMENTAL SET-UP AND REMIND OF THE STATIC DISPLACEMENT SELF-MEASUREMENT

The experimental platform including the 2-DOF piezoactuator is described in this section with a brief remind of the related static self-measurement.

A. The experimental setup

The proposed actuator, is a 2-DOF piezoactuator with a rectangular cross-section. The actuators integrates 2 piezoelectric layers and 5 electrodes. A full description of the actuator design and working principle can be found in [22].

The experimental setup (Fig. 1) includes:

- The 2-DOF piezoactuator itself. Its active dimensions are: $22mm \times 1mm \times 0.91mm$.
- Two optical displacement sensors which are used to measure the deflection of the actuator in each axis y and z. The sensors were installed within acceptable range away from the target (actuator) to measure the bending at its tip. The sensors measurements are employed in order to characterize the actuator and to verify the effectiveness of the proposed 2-DOF self-measurement. Hence the sensors are not used for the feedback control, but to verify the efficiency of the feedback which uses the self-measurement. The sensors, LC2420 from *Keyence* company, have resolution of $40nm$ and bandwidth of $2kHz$.
- Four identical electrical circuits which was fabricated with a configuration illustrated in Fig. 2. Each circuit includes 2 capacitance, low-bias current Op-Amp and resistance [22]. This circuit is used to amplify and to

transform the electrical charges appearing on the piezo-electric electrodes into exploitable voltage.
- And a dSPACE ControlDesk (dS1103) data acquisition board with a computer (PC). The whole acquisition system is used to generate the driving voltage for the piezoactuator, to acquire the signals from the electrical circuit, and to implement the 2-DOF dynamic observer as well as the further H_∞ feedback controller. MATLAB-Simulink software is employed for the implementation. The sampling frequency is set to $5kHz$ which is much sufficient for the experimental tests carried out.

B. Remind of static displacement self-measurement of 2-DOF piezoactuator

Applying an input voltage U to a single degree of freedom unimorph or multimorph piezoelectric cantilever actuator of a geometry: length L_o, width w_o and thickness h_o contributes a deflection δ_o as well as an electric charge Q that will appear on the surface/electrodes of the actuator. This resulting electrical charge can be amplified and transformed into exploitable voltage U_o using an external electrical circuit. The relation between the applied input voltage and the contributed charge can be expressed as a function of the geometrical properties of the actuator and the dielectric coefficient ε_{33}^S as $Q = \frac{4w_o L_o \varepsilon_{33}^S}{h_o} U_{in}$. The deflection can be linearly related to the charge Q as $\delta_o = Q/\gamma$, where γ is the actuator charge-displacement coefficient [23].
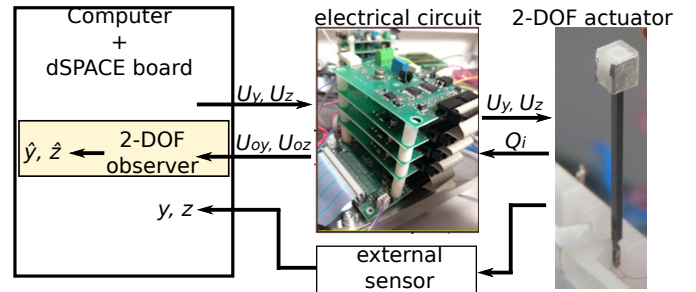

Fig. 1: Schematic of the experimental platform.

For the 2-DOF piezoactuator which exhibits four potential electrodes and one common ground, there are four electrical charge Q_i to be amplified and to be exploited. Thus, the electrical circuit in is repeated four times [22]. Fig. 2-a depicts the general diagram of the static self-measurement [22]. The exploitable voltages U_{oi} ($i \in \{1, 2, 3, 4\}$) from the electrical circuit as well as the driving voltages U_y and U_z are considered as the available signals to the (static) observer in order to provide static estimation $\hat{y}_s$ and $\hat{z}_s$ of the real displacements y and z at their steady-state regime (y_s and z_s). By static, we mean that the self-measurement provides precise estimation when the signal are constants or low-frequency. At high frequency or for transient part of a step-response, the estimation is not precise. However, for feedback control application, having static estimation is not sufficient.

In the next section, we therefore introduce a dynamic observer to the existing static self-measurement in order to permit a dynamic self-measurement of the displacement of the 2-DOF piezoactuator. For a further reading regarding the static observer, more details on its developments and parameters identification are available at [22].
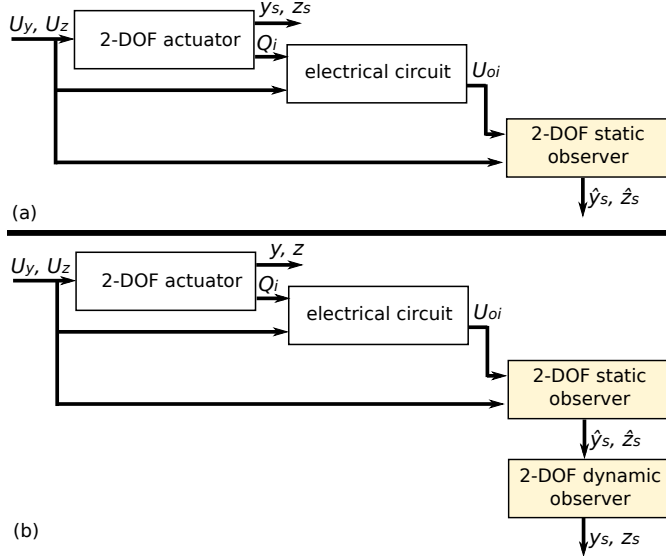

Fig. 2: (a): the static self-measurement [22]. (b): the suggested dynamic self-measurement.

III. EXTENSION TO A DYNAMIC SELF-MEASUREMENT

The previous static observer is extended into dynamic observer in this section in order to provide an estimate displacement of the 2-DOF actuator in various regimes: static, low frequency and high frequency. As displayed in Fig. 2-b, the general principle consists in using all available signals so far as information for the dynamic observer such that the latter reconstructs and provides the complete (static and dynamic) information regarding the output displacement. The available signals are the driving voltage U_y and U_z and the estimate static displacement $\hat{y}_s$ and $\hat{z}_s$

A. Synthesizing the 2-DOF displacement dynamic observer

Both the static and dynamic regimes of the output displacement $y(t)$ and $z(t)$ of the actuator are well estimated if the following conditions are satisfied:

$$\begin{cases} \hat{y}(t) = y(t), & \forall t \in \mathbb{R}^+, \\ \hat{z}(t) = z(t), & \forall t \in \mathbb{R}^+. \end{cases} \tag{1}$$

Eq. 1 can be represented in the Laplace domain as:

$$\begin{cases} \hat{y}(s) = y(s); & \forall s \in \mathbb{C}, \\ \hat{z}(s) = z(s); & \forall s \in \mathbb{C}. \end{cases} \tag{2}$$

The formulation of the complete 2-DOF displacement observer of the actuator requires a 2-DOF model of the piezoactuator that can describe the output displacement properties of the actuator along each axis. Considering a linear behavior

and considering that there is no external force applied to the actuator, the measured output displacement $y(s)$ and $z(s)$ can be related to the associated applied voltage U_y and U_z as:

$$\begin{cases} y(s) = d_y D_y(s) U_y(s) + d_{yz} D_{yz}(s) U_z(s), \\ z(s) = d_{zy} D_{zy}(s) U_y(s) + d_z D_z(s) U z(s), \end{cases} \tag{3}$$

where $D_y(s)$ and $D_z(s)$ are the normalized dynamics of the actuator in the direct transfers and $D_{yz}(s)$ and $D_{zy}(s)$ are the normalized dynamics of the actuator in the cross-couplings transfers. We have $D_k(s = 0) = 1$, $\forall k \in \{y, z, yz, zy\}$. The parameters d_k are the static gains. It is worth to note that the hysteresis and the creep nonlinearities were neglected in this case which limits the self-measurement to low voltage applications. Ongoing works extend this work in order to account for these nonlinearities. It is also worth to note that the above model accounts for the cross-couplings, which is essential in multi-DOF actuators.

Let us denote $\Delta_k(s)$, $\forall k \in \{y, z, yz, zy\}$, the content of the dynamic observer such that:

$$\begin{cases} \hat{y}(s) = \Delta_y(s)\hat{y}_s(s) + \Delta_{yz}(s)\hat{z}_s(s), \\ \hat{z}(s) = \Delta_{zy}(s)\hat{y}_s(s) + \Delta_z(s)\hat{z}_s(s). \end{cases} \tag{4}$$

Remind that $\hat{y}_s$ and $\hat{z}_s$ represent the estimate static value of y and of z respectively and which is provided by the existing static self-measurement.

Remind also that the (real) static displacement is obtained from the dynamic model in Eq. 3 by letting $D_k(s = 0) = 1$, that is:

$$\begin{cases} y_s(s) = d_y U_y(s) + d_{yz} U_z(s), \\ z_s(s) = d_{zy} U_y(s) + d_z U_z(s). \end{cases} \tag{5}$$

Consequently, assuming a perfect static observer and self-measurement from Fig. 2-b and from [22], i.e. $\hat{y}_s = y_s$ and $\hat{z}_s = z_s$, we could derive from Eq. 5 that:

$$\begin{cases} \hat{y}_s(s) = d_y U_y(s) + d_{yz} U_z(s), \\ \hat{z}_s(s) = d_{zy} U_y(s) + d_z U_z(s). \end{cases} \tag{6}$$

Note that the conditions $\hat{y}_s = y_s$ and $\hat{z}_s = z_s$ require the electrical circuit to have a bandwidth superior to that of the piezoactuator.

Replacing $\hat{y}_s$ and $\hat{z}_s$ in Eq. 4 with Eq. 6, we obtain the dynamic observer equation:

$$\begin{cases} \hat{y}(s) = \Theta_y(s) U_y(s) + \Theta_{yz}(s) U_z(s), \\ \hat{z}(s) = \Theta_{zy}(s) U_y(s) + \Theta_z(s) U_z(s), \end{cases} \tag{7}$$

where

$$\begin{cases} \Theta_y(s) = d_y \Delta_y(s) + d_{zy} \Delta_{yz}(s), \\ \Theta_{yz}(s) = d_{yz} \Delta_y(s) + d_z \Delta_{yz}(s), \\ \Theta_{zy}(s) = d_y \Delta_{zy}(s) + d_{zy} \Delta_z(s), \\ \Theta_z(s) = d_{yz} \Delta_{zy}(s) + d_z \Delta_z(s), \end{cases} \tag{8}$$

In order to satisfy the objective of dynamic self-measurement in Eq. 2, we should have the observer equation in Eq. 7 equal to the dynamic model in Eq. 3, i.e.:

$$\begin{cases} \Theta_y(s) = d_y D_y(s), \\ \Theta_{yz}(s) = d_{yz} D_{yz}(s), \\ \Theta_{zy}(s) = d_{zy} D_{zy}(s), \\ \Theta_z(s) = d_z D_z(s), \end{cases} \quad (9)$$

From Eq. 8 and Eq. 9, the observer parameters are therefore derived:

$$\begin{cases} \Delta_y(s) = \frac{d_{zy} d_z}{(d_y d_z - d_{yz} d_{zy})} \left(\frac{d_y}{d_{zy}} D_y(s) - \frac{d_{yz}}{d_z} D_{yz}(s) \right), \\ \Delta_{yz}(s) = \frac{d_y d_{yz}}{(d_{yz} d_{zy} - d_y d_z)} \left(D_y(s) - D_{yz}(s) \right), \\ \Delta_{zy}(s) = \frac{d_{zy} d_z}{(d_y d_z - d_{yz} d_{zy})} \left(D_{zy}(s) - D_z(s) \right), \\ \Delta_z(s) = \frac{d_y d_{yz}}{(d_{zy} d_{yz} - d_y d_z)} \left(\frac{d_{zy}}{d_y} D_{zy}(s) - \frac{d_z}{d_{yz}} D_z(s) \right), \end{cases} \quad (10)$$

B. Experimental validation of the 2-DOF dynamic self-measurement

The transfer functions $d_k D_k(s)$, $\forall k \in \{y, z, yz, zy\}$, have been identified using step responses of the 2-DOF actuator under input of 5 V. The measured data was afterwards used to identify the transfer function. The systems identification toolbox in MATLAB [24]. The ARMAX technique (Auto Regressive Moving Average with eXternal inputs) was applied for that. We obtain,

$$\begin{cases} d_y = 5.6 \mu m/V, \\ D_y(s) = \frac{989.98(s^2 - 440.25s + 4.976 \times 10^7)}{(s+4894)(s^2 + 48.22s + 1.005 \times 10^7)}, \end{cases} \quad (11)$$

$$\begin{cases} d_z = 5.01 \mu m/V, \\ D_z(s) = \frac{670(s^2 + 2554s + 5.092 \times 10^7)}{(s+4367)(s^2 + 44.87s + 7.82 \times 10^6)}, \end{cases} \quad (12)$$

$$\begin{cases} d_{yz} = 0.08 \mu m/V, \\ D_{yz}(s) = \frac{-87(s+3.2 \times 10^4)(s+1.8 \times 10^4)}{(s+4894)(s^2 + 48s + 1 \times 10^7)}, \end{cases} \quad (13)$$

and

$$\begin{cases} d_{zy} = 0.29 \mu m/V, \\ D_{zy}(s) = \frac{-1591(s^2 + 2002s + 1.1 \times 10^7)}{(s+2227)(s^2 + 60.8s + 7.9 \times 10^6)}, \end{cases} \quad (14)$$

The dynamic observer has been implemented additionally to the existing static self-measurement by following Fig. 2-b. Then, step responses tests have been carried out to verify the efficiency of the whole dynamic self-measurement. Fig. 3 depicts the results when step voltages with amplitudes of $U_y = 5V$ and $U_z = 5V$ are applied successively. Fig. 3-a (resp. Fig. 3-d) show that the estimate displacement $\hat{y}$ (resp. $\hat{z}$) from the observer well coincides with the real output displacement y (resp. z) measured by the external optical sensor, both in its transient regime (dynamic) and its steady-state regime (static). Furthermore, Fig. 3-b (resp. Fig. 3-c) shows that the cross-couplings observed at y (resp. z) and due to U_z (resp. U_y) is also conveniently estimated by the dynamic observer and its self-measurement. It is worth to note that the observer does not contain real-time correction such as Luenberger observer.

Hence, the model used to construct the obsrever should be as precise as possible.
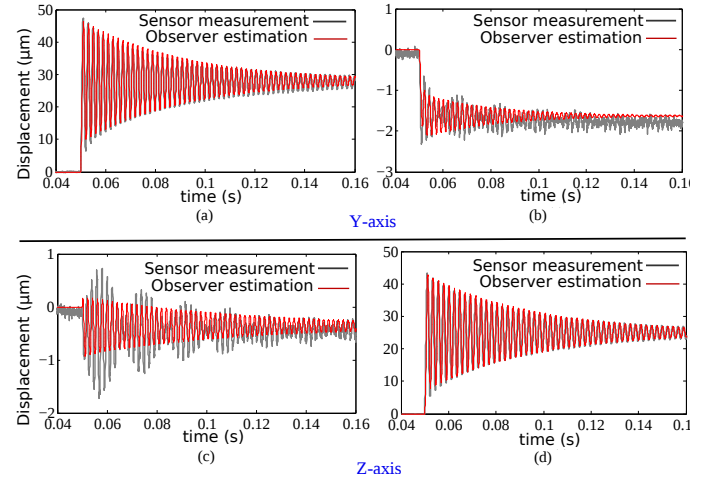

Fig. 3: Step responses of the 2-DOF actuator when applying $5V$ of amplitudes: comparison between the estimated output displacement and the real displacement measured by the optical sensors.

IV. APPLICATION OF THE DYNAMIC SELF-MEASUREMENT TO A H_∞ FEEDBACK CONTROL DESIGN

The output of the proposed self-measurement observer for the 2-DOF piezoactuator is employed in this section as a feedback of an H_∞ controller. The controller is designed to reject the cross-couplings and to have certain tracking performances.

A. Remind of the model to be controlled

The system to be controlled includes: the 2-DOF piezoactuator, the electrical circuit, the static observer and the dynamic observer designed in this paper. This new system has inputs U_y and U_z and outputs $\hat{y}$ and $\hat{z}$. Fig. 4-a depicts the new system and the feedback controllers $C_y(s)$ and $C_z(s)$ to be synthesized. In the figure, y_{ref} and z_{ref} are the reference inputs.

It is clear that, when the self-measurement and its dynamic observer well estimates the real displacement, we can assume that the model of the new system is similar to that of the model in Eq. 3, that is:

$$\begin{cases} \hat{y}(s) = d_y D_y(s) U_y(s) + d_{yz} D_{yz}(s) U_z(s), \\ \hat{z}(s) = d_{zy} D_{zy}(s) U_y(s) + d_z D_z(s) U_z(s), \end{cases} \quad (15)$$

i.e.

$$\begin{cases} \hat{y}(s) = G_y(s) U_y + p_y(s), \\ \hat{z}(s) = G_z(s) U_z + p_z(s), \end{cases} \quad (16)$$

where $G_y(s) = d_y D_y(s)$ and $G_z(s) = d_z D_z(s)$, and where $p_y(s) = d_{yz} D_{yz}(s) U_z(s)$ and $p_z(s) = d_{zy} D_{zy}(s) U_y(s)$ are

internal disturbance due to the cross-couplings. From the model in Eq. 16, the initial 2-DOF system with dynamic self-measurement is equivalent to two single-input-single-output (SISO) systems with disturbance. Fig. 4-b is therefore the equivalent scheme of Fig. 4-a
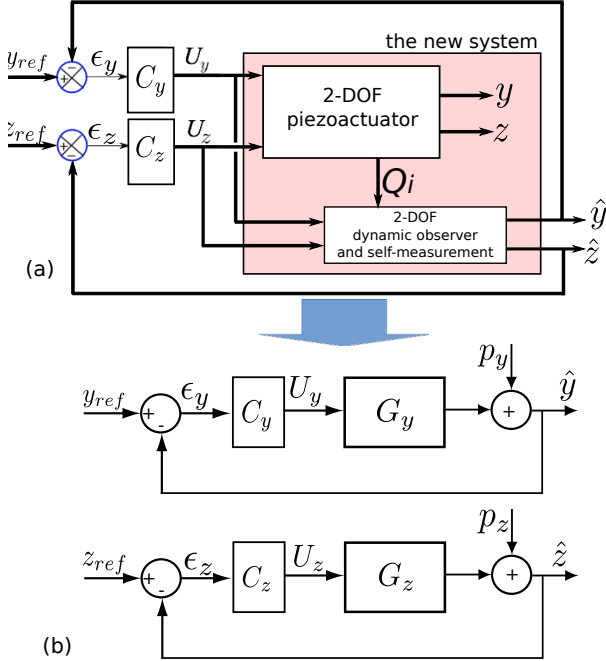

Fig. 4: (a): closed-loop block diagram. (b): equivalent scheme.

B. Specifications

In order to match with precise positioning requirements, we choose the following specifications for the closed-loop.

Tracking performance - The specification here is to ensure reference tracking performance. It is taken to be similar for y and z axes. The specifications choice is based on the fact that the direct transfers responses in Fig. 3-a and d) should be improved in the closed loop: no vibration anymore and reduced settling time. We therefore choose as follows.

- The static error should be less than 1%.
- The overshot percentage which is nearly 69% along y axis and 68% along z axis (see Fig. 3-a and -d) should be 0 for the closed-loop.
- The settling time along both axes should not exceed 15ms.

Input voltage limitation - The specification here, also called command moderation, is to ensure that the voltage applied to the actuator does not exceed certain values. In particular, the following values have been chosen to not exceed the displacement per voltage gain that we found during the characterization (see the steady-state values of the step response in Fig. 3-a and -d).

- For the y axis, the maximum ratio is imposed to be $\frac{U_{ymax}}{y_{max}} = \frac{5V}{29\mu m} = 0.1786[\frac{V}{\mu m}]$.

- For the z axis, the maximum ratio $\frac{U_{zmax}}{z_{max}} = \frac{5V}{25\mu m} = 0.1996[\frac{V}{\mu m}]$.

Each of this gain was used as command moderation specification for y and for z axis respectively.

Disturbance rejection - The disturbance is principally due to the cross-couplings p_y and p_z. We suggest here to account for them in the controller synthesis. Fig. 3-b shows that the affect of U_z on $\hat{y}$ reaches $p_{y-max=2.48\mu m}$ (maximal overshot) and Fig. 3-c shows that the affect of U_y on $\hat{z}$ reaches $p_{z-max=1.88\mu m}$ (maximal overshot), in absolute values. Let us take the worst case of $2.48\mu m$ for both axes. Thus, the specification of disturbance rejection for both axes is:

- No overshot in the response $\hat{y}$ (resp. $\hat{z}$) when a step reference z_{ref} (resp. y_{ref}) is applied to the closed-loop.
- A disturbance of $2.48\mu m$ should not affect the output more than $0.3\mu m$ ($\frac{0.3}{2.48} = 12\%$): $\frac{\epsilon_y}{p_{y-max}} = \frac{\epsilon_z}{p_{z-max}} = 12\%$ in steady-state regime (static error).
- Finally, the maximum settling time to reject the disturbance should not exceed $9ms$.

C. Standard H_∞ controller design

The desired specifications that were suggested in the previous section can be achieved by employing weighting functions. The technique is explained here for y axis which is similar for z axis.

The tracking performance specification is considered by introducing a weighting function $W_1(s)$ to the error signal ϵ_y. A weighting function $W_2(s)$ applied to the voltage U_y accounts for the command moderation specification. Finally, a weighting function W_3 is put in the disturbance p_y in order to consider its rejection by the controller to be calculated. Notice that, since the numerical values of the specifications are the same for y and z axes, the same weighting functions apply for both of them, as displayed in the augmented closed-loop diagram in Fig. 5-a. The augmented diagram is only used to synthesize the controller. The weightings are removed when implementing this latter. In the figure, e_{y1} and e_{y2} (resp. e_{z1} and e_{z2}) are the weighted outputs and b_y (resp. b_z) is the new input related to the disturbance for the y axis (resp. z axis).

Fig. 5-b illustrates the standard scheme derived from the augmented closed-loop for the y axis in Fig. 5-a. This standard scheme relates the augmented system $\mathcal{P}_y(s)$ with the controller $C_y(s)$ and is used for the standard H_∞ problem.

Problem (Pbl.1) - the standard H_∞ approach: The objective is to seek the controller $C_y(s)$ such that:

- The interconnection of Fig. 5-b is stable.
- The lower linear fractional transformation (LFT) $F_{yl}(\mathcal{P}_y(s), C_y(s))$, which is defined as the transfer function bewteen exogenous signals $(e_{y1}, e_{y2})^T$ and $(y_{ref}, b_y)^T$ in presence of the interconnection with $C(s)$, is such that
$$||F_{yl}(\mathcal{P}_y(s), C_y(s))||_\infty < \gamma_y .$$

In our case, this LFT function $F_{yl}(\mathcal{P}_y(s), C_y(s))$ can be represented in matricial function as:
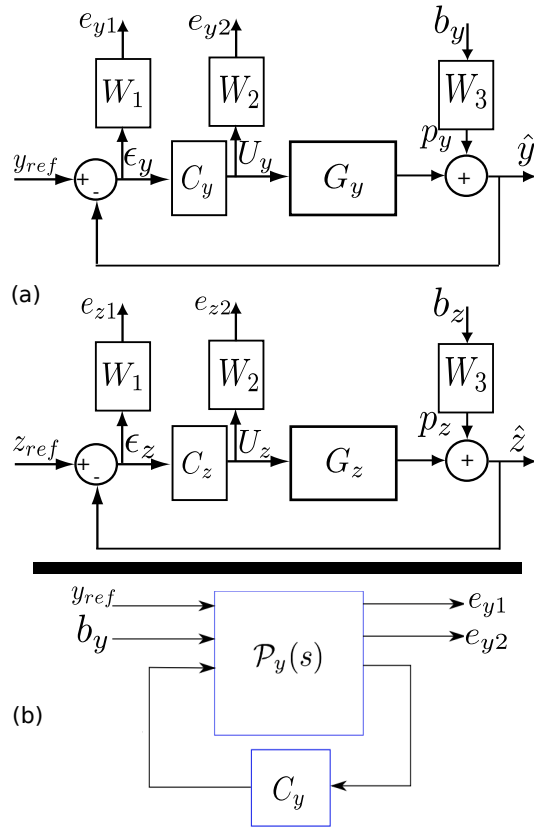
Fig. 5: (a): the augmented closed-loop scheme with weightings. (b): the standard scheme for y axis.

$$\left(\begin{array}{c} e_{y_1} \\ e_{y_1} \end{array} \right) = F_{yl}(\mathcal{P}_y(s), C_y(s))\left(\begin{array}{c} y_{ref} \\ b_y \end{array} \right). \tag{17}$$

For a sensitivity function $S_y(s)$ and a complementary sensitivity function $H_y(s) = S_y C_y G_y$ such that:

$$S_y(s) = \frac{\epsilon_y(s)}{y_{ref}(s)} = \frac{1}{1 + C_y G_y}, \tag{18}$$

we have:

$$F_{yl}(\mathcal{P}_y(s), C_y(s)) = \left(\begin{array}{cc} W_1 S_y & -W_1 S_y W_3 \\ W_2 C_y S_y & -W_2 C_y S_y W_3 \end{array} \right). \tag{19}$$

From the standard H_∞ problem above, we should calculate the controller $C_y(s)$ such that:

$$\left\| \left(\begin{array}{cc} W_1 S_y & -W_1 S_y W_3, \\ W_2 C_y S_y & -W_2 C_y S_y W_3 \end{array} \right) \right\|_\infty < \gamma_y, \tag{20}$$

i.e.

$$\|W_1 S_y\|_\infty < \gamma_y, \quad \|-W_1 S_y W_3\|_\infty < \gamma_y, \tag{21}$$
$$\|W_2 C_y S_y\|_\infty < \gamma_y, \|-W_2 C_y S_y W_3\|_\infty < \gamma_y,$$

which is also satisfied if we have:

$$|S_y| < \gamma_y|\frac{1}{W_1}|, \quad |-S_y| < \gamma_y \frac{1}{W_1 W_3}, \tag{22}$$
$$|C_y S_y| < \gamma_y|\frac{1}{W_2}|, \quad |-C_y S_y| < \gamma_y, \frac{1}{W_2 W_3}.$$

In these latter conditions, i.e. Ineq. 22, $\frac{1}{W_1}$ is called (frequency domain) gabarit for the tracking performance specification since it is used to impose bound and shape for $S_y(s)$ in its frequency domain. On the other hand, $\frac{1}{W_2}$ is the gabarit for the command moderation specification and $\frac{1}{W_1 W_3}$ is gabarit for the disturbance rejection specification. The weighting functions W_1, W_2 and W_3 are derived by matching these gabarits with the specifications described in section-IV-B. For that, we suggest the following gabarits structures for the tracking performance:

$$\frac{1}{W_1} = \frac{k_o s + \frac{3\epsilon_s}{t_r}}{s + \frac{3}{t_r}} = \frac{s+2}{s+200}, \tag{23}$$

where $k_o = 1$ means that there is no overshot, and where $\epsilon_s = 1\%$ is the desired maximal statical error and $t_r = 15ms$ is the desired maximal response time (see section-IV-B).

For the command moderation specification, a simple gain can be used as bound:

$$\frac{1}{W_2} = 0.1786[\frac{V}{\mu m}], \tag{24}$$

Finally, for the disturbance rejection, teh structure and the derivation of the gabarit are similar to those of the tracking performance ones. We have:

$$\frac{1}{W_1 W_3} = \frac{s+40}{s+333}. \tag{25}$$

Notice that the coefficient γ_y, called performance level, should be as small as possible. If $\gamma_y \leq 1$, the specified performances will be guaranteed by the controller. However if $\gamma_y > 1$, it is not guaranteed that the performances will be satisfied.

D. Calculation of the controllers

To solve the H_∞ problem in Pbl.1 (stability and bound of the gain) and, thus in our case, to find the controller $C_y(s)$ such that Ineq. 22 is satisfied, the Glover-Doyle algorithm [25] has been applied. The resolution in this algorithm is based on the Riccati equations and it uses the dichotomy technique to find the optimal value of γ_y. The same principle used for $C_y(s)$ was also applied for $C_z(s)$. We obtain:

$$\begin{cases} \gamma_{y-opt} = 1.6, \\ C_y(s) = \frac{3823(s+4894)(s+200)(s+23)(s^2+48s+1e7)}{(s+3.9e4)(s+2)(s^2+158s+2.4e4)(s^2+6029s+3.6e7)} \end{cases} \tag{26}$$

and

$$\begin{cases} \gamma_{z-opt} = 1.8, \\ C_z(s) = \frac{1593(s+4367)(s+200)(s+24)(s^2+45s+7.8e6)}{(s+1.3e4)(s+2)(s^2+135s+3.4e4)(s^2+5092s+2.1e7)}, \end{cases}$$

(27)

where $e\nu = \times 10^{\nu}$, for example: $3.6e7 = 3.6 \times 10^7$.

Notice that the optimal values of γ for each controller exceed one: $\gamma_{y-opt} = 1.6$ and $\gamma_{z-opt} = 1.8$. Although the specified performances may not be ensured, the deviance should be very light because these γ values are still low.

E. Experimental results

The calculated controllers $C_y(s)$ and $C_z(s)$ were implemented in MATLAB-Simulink environment and applied to the setup by following Fig. 4.

First, step references of $y_{ref} = 20\mu m$ and $z_{ref} = 20\mu m$ were applied simultaneously. The objective is to check if the specifications are satisfied despite the cross-couplings that should occur in the y axis (resp. z axis) due to z_{ref} (resp. y_{ref}). Fig. 6 depicts the results. It clearly shows that the specified settling time (less than $15ms$), the overshot (0%) and the static error (less than 1%) are correctly satisfied for both axes, with the presence of disturbance (which is the effect of the other axis). Notice that the fact that the response along z axis exhibits slightly higher settling time than that of y axis is due to the specification imposed to be similar for both. Indeed, during the command moderation specifications in section-IV-B, we used the worst case which corresponded to the gain for y axis. Hence, the response along z axis requires more effort, which here is represented by a higher settling time.
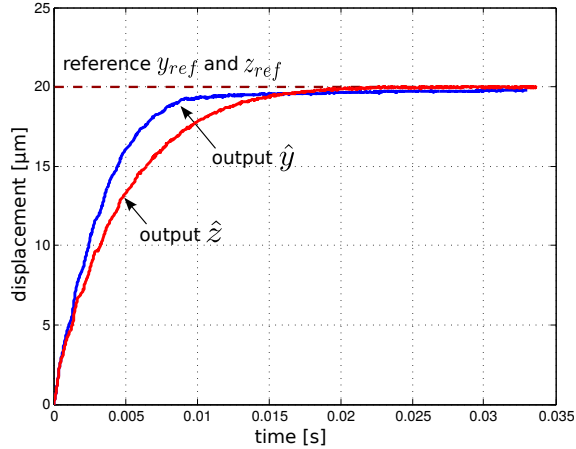

Fig. 6: Step responses of the closed-loop by applying $y_{ref} = 20\mu m$ and $z_{ref} = 20\mu m$ simultaneously.

The next experiment consists in performing the frequency response of the closed-loop, for each axis independently. Fig. 7 depicts the results. They show that the bandwidth is of $96Hz$ for the $\hat{y}$ axis and of $80Hz$ for the $\hat{z}$ axis which are important in applications such as micromanipulation [2].
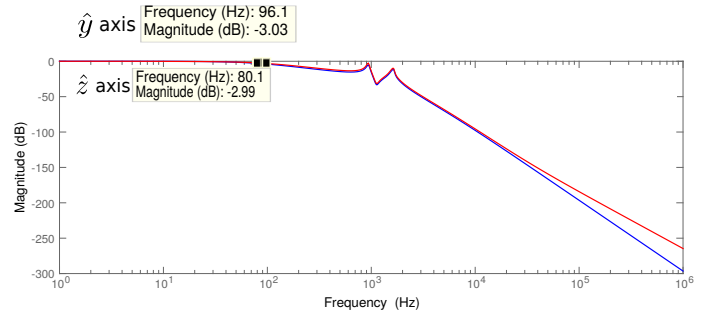

Fig. 7: Frequency responses of the closed-loop.

The last tests consist in applying a circular spatial trajectory reference to the closed-loop. To this aim, the individual reference is given by: $y_{ref} = 20\mu m \sin(2\pi f t)$ and $z_{ref} = 20\mu m \cos(2\pi f t)$, where the frequency is chosen to be $f = 10Hz$. Fig. 8 depicts the result which demonstrates that the closed-loop system well tracks the complex trajectory. As a measure of performances, we use the spatial error given by: $\varepsilon = \left(\sqrt{y_{ref}^2 + z_{ref}^2} - \sqrt{\hat{y}^2 + \hat{z}^2} \right)$. We found that the maximal absolute error is $|\varepsilon| = 2.1\mu m$, which in relative value is $\frac{|\varepsilon|}{40\mu m} \approx 5\%$. This is a good result for applications such as micromanipulation, in particular with such trajectory frequency ($10Hz$). However when the frequency is increased, the error starts to increase due to the phase-lag first (beyond $30Hz$ for both axes), and also due to the bandwidth of the closed-loop system (beyond $96Hz$) and $80Hz$ respectively). The error could be limited by introducing the type of reference signal (for eg. circular trajectory) and its operating frequency in the specifications used to calculate the controller in order to decrease this error.

For comparison, we also applied the self-measurement and feedback control developed in [18]. The technique in this previous work was valid for only 1-DOF piezoactuators. The test consists therefore in applying this 1-DOF self-measurement and feedback control to each of the y and z axis of our 2-DOF piezoactuator. The experimental results show that, with the same condition than above (circular trajectory with $10Hz$ of frequency and $20\mu m$ of amplitude), the absolute error is of 15% which is much larger than that from the technique suggested in this paper. This is due to the fact that the observer technique inside the self-measurement developed in [18] does not consider cross-couplings. Hence, once the reference input involves the two axes y and z simultaneously, the error drastically increases.

V. CONCLUSION AND PERSPECTIVES

The work reported in this paper consisted in suggesting an embedded measurement technique capable of measuring both low and high frequency regimes of the displacement in a 2-DOF piezoelectric actuator. For this aim, a dynamic 2-DOF observer was synthesized to estimate the dynamic output displacement of the actuator which was equipped with static self-measurement technique. Beyond the dynamics, the observer was also able to track the cross-couplings between
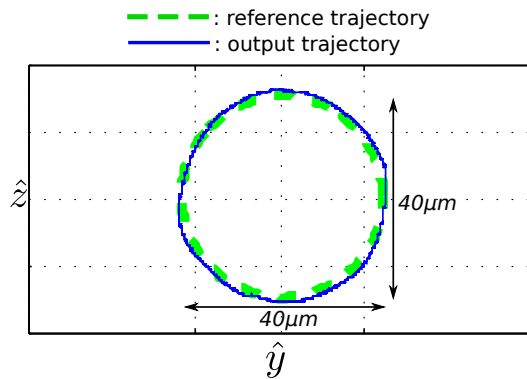
Fig. 8: Circular trajectory tracking of the closed-loop.

the two axes of the actuator. Then, the output of the observer was used as a feedback for a H_∞ controller. The dynamic measurement as well as the feedback control were verified experimentally and gave maximal closed-loop tracking error of 1% as well as settling time better than $15ms$ and bandwidth in excess of $80Hz$

The linear observer for self-measurement developed in this paper is valid for small displacement of the 2-DOF piezoactuator. Ongoing works consist in extending the observer into nonlinear such that hysteresis and creep are accounted for and thus estimation and feedback controll with large displacement condition will be possible.

REFERENCES

[1] A. Bergander, W. Driesen, T. varidel, M. Meizoso and J. M. Breguet, 'Mobile cm3-microrobots with tools for nanoscale imaging and micro-manipulation', Mechatronics & Robotics, pp.1041-1047, Sept 2004.
[2] J. Agnus, et al., 'Robotic microassembly and micromanipulation at FEMTO-ST', Journal of Micro-Bio Robotics, vol.8(2), pp.91-106, 2013.
[3] N. Dechev, W. L. Cleghorn and J. K. Mills, 'Microassembly of 3-D MEMS structures utilizing a MEMS microgripper with a robotic manipulator', Int. Conference on Robotics and Automation, pp.3193-3199, Taipei, Taiwan, 2003.
[4] G. Bining, C. F. Quate and C. Berger, 'Atomic Force Microscope', APS Physical Review Letters, vol.56(9), pp. 930-933, 1986.
[5] E. Grochowski and R.F. Hoyt, 'Future Trends In Hard Disk Drives', IEEE transactions on Magnetics, 32(3), pp. 1850-1854, 1996.
[6] S. Devasia, E. E. Eleftheriou, R. Moheimani, 'A survey of control issues in nanopositioning', IEEE Transactions on Control Systems Technology, Vol.15(15), pp.802-823, 2007.
[7] M. Rakotondrabe, 'Smart materials-based actuators at the micro/nano-scale: characterization, control and applications', edited book, Springer - Verlag, New York, ISBN 978-1-4614-6683-3, 2013.
[8] M. Al Janaideh and P. Krejci, 'Inverse rate-dependent Prandtl-Ishlinskii model for feedforward compensation of hysteresis in a piezomicropositioning actuator', IEEE/ASME Transactions on Mechatronics, vol.18(5), pp.1498-1507, 2013.
[9] M. Rakotondrabe, 'Multivariable classical Prandtl-Ishlinskii hysteresis modeling and compensation and sensorless control of a nonlinear 2-dof piezoactuator', Nonlinear Dynamics, DOI: 10.1007/s11071-017-3466-5, 2017.
[10] B. Mokaberi and A. A. G. Requicha, 'Compensation of scanner creep and hysteresis for AFM nanomanipulation', IEEE Transactions on Automation Science and Engineering, pp.197-208, 2008.
[11] D. Croft, G. Shed and S. Devasia, 'Creep, hysteresis and vibration compensation for piezoactuators: atomic force microscopy application', ASME Journal of Dynamic Systems, Measurement and Control, 2001.
[12] M. Rakotondrabe, 'Modeling and Compensation of Multivariable Creep in multi-DOF Piezoelectric Actuators', IEEE Int. Conference on Robotics and Automation, pp.4577-4581, St Paul Minnesota USA, 2012.
[13] J. J. Doschm D.I. Inman and E. Garcia, 'A Self-Sensing Piezoelectric Actuator for collocated Control', Journal of Intell. Mater. Syst. and Struct, vol.3, pp.166-185, 1992.
[14] T. Takigami, K. Oshima, Y. Hayakawa and M. Ito "Application of Actuator to cof a soft-handling gripper ", Journal Proc. to IEEE ICCA , pp. 902-906, Italy, 1998.
[15] E. Anderson, N. Hagood anf J. Goodliffef, 'Self-sensing piezoelectric actuation - Analysis and application to controlled structures', 33rd Structures, Structural Dynamics and Materials Conference, April.
[16] P. C. Khiang, G. Guo, M. B. Chen, T. H. Lee, 'Self-sensing actuation for nanopositioning and active-mode damping in dual-stage HDDs', IEEE/ASME Transactions on Mechatronics, vol.11(3), pp.328,338, June 2006
[17] Y. Cui, 'Compounding Control of Piezoceramic Micro-Motion Worktable Based on Integrator', World Congress on Intell. Cont. and Autom., China, 2006.
[18] M. Rakotondrabe, A. Ivan, S. Khadraoui, P. Lutz and N. Chaillet, 'Simultaneous displacement and force self-sensing in piezoelectric actuators and applications to robust control of the displacement', IEEE/ASME Transactions on Mechatronics, vol.20(2), Jan. 2014.
[19] M. Rakotondrabe, 'Combining self-sensing with an Unkown-Input-Observer to estimate the displacement, the force and the state in piezoelectric cantilevered actuator', American Control Conference, pp.4523-4530, Washington DC USA, June 2013.
[20] I. A. Ivan, M. Rakotondrabe, P. Lutz, and N. Chaillet, 'Quasi-static displacement self-sensing method for cantilevered piezoelectric actuators', Review of Scientific Instruments, Vol.80(6), 065102, June 2009.
[21] E. Grasso, N. Totaro, H. Janocha and D. Naso, 'Piezoelectric self sensing actuators for high voltage excitation.' Smart Mater. Struct. 22, 065018, 2013.
[22] I. A. Ivan, O. Aljanaideh, J. Agnus, P. Lutz and M. Rakotondrabe, 'Quasi-static displacement self-sensing measurement for a 2-DOF piezoelectric cantilevered actuator', IEEE Transactions on Industrial Electronics, vol.64(8), pp. 6330-6337, Aug. 2017.
[23] J.G. Smits, and W. S. Choi, 'The constituent equations of piezoelectric heterogeneous bimorphs', IEEE Transactions on Ultrasonics, Ferroelectrics, and Frequency Control, vol.38(3), pp.256,270, May 1991.
[24] L. Ljung, 'System identification toolbox', The Matlab user's guide, 1988.
[25] J.C. Doyle, K. Glover, P.P. Khargonekar, B.A. Francis, 'State-space solutions to standard H-2 and H-inf control problems', IEEE Transactions on Automatic Control, vol.34(8), pp.831-847, 1989.